

# Force Error Optimization in Smooth Particle Hydrodynamics

<sup>1</sup>R. Capuzzo–Dolcetta, <sup>1,2</sup>R. Di Lisio

<sup>1</sup> *Istituto Astronomico*  
*Università di Roma “La Sapienza”*  
*Via G.M. Lancisi 29*  
*I-00161 Roma*

<sup>2</sup> *Dipartimento di Matematica*  
*Università di Roma “La Sapienza”*  
*P.le Aldo Moro 5*  
*I-00185 Roma*

Subject classification: 65C20, 76M25

Keywords: particle numerical-methods, compressible fluid-dynamics.

**Abstract** We discuss capability of Smooth Particle Hydrodynamics to represent adequately the dynamics of self-gravitating systems, in particular for what regards the quality of approximation of force fields in the motion equations. When cubic spline kernels are used, we find that a good estimate of the pressure field cannot be obtained in non uniform situations using the commonly adopted scheme of adapting the kernel sizes to include a fixed number of neighbours. We find that a fixed number of neighbours gives the best approximation of just the intensity of the force field, while the determination of the direction of the force requires a number of neighbours which strongly depends on the particle position. A good balance between quality of the approximation and computer time consumption is obtained assuming the latter about 2 times larger than the first one. We suggest a procedure which is massively parallelizable. With a suitable choice of the kernel sizes the amount of computations required is less than twice the one required by the common SPH scheme at the same level of approximation, so our recipe (when parallelized) is convenient.

## 1. Introduction

The subject of this paper is a numerical technique which is largely used in fluid-dynamical simulations: the so called Smooth Particle Hydrodynamics (SPH).

This particle method was firstly introduced by Lucy [1] and Gingold and Monaghan [2] to simulate nonaxisymmetric fluids in Astrophysics, and it became popular due to its robustness and easy implementation.

Basically, the idea of the method is to consider the fluid as an ensemble of (smooth) particles, anyone being representative of a piece of fluid. In this scheme, each particle is mathematically characterized by a “kernel” (a symmetric, regular non-negative function centered on the particle position) which carries information on the average values of dynamical and thermodynamical quantities, as well as on their gradients. The size of the kernel may depend on the local density of the particles.

Each particle moves in the force field generated by the whole particle system, while the associated quantities evolve under their suitably regularized laws (a more detailed description of this method can be found in [3]).

It is well known that necessary requirements for a good numerical method are compatibility with “analytical” equations, convergence to the right solutions and stability. At present, these properties have not yet been completely

proved for SPH. Few results are available; for instance Oelschläger [4] and Di Lisio [5] have obtained convergence results for a particular equation of state (EOS),  $P \propto \rho^2$ , in the free and self-gravitating cases, respectively.

A more general convergence result, for a freely moving polytropic compressible fluid, can be found in Di Lisio, Grenier, Pulvirenti [6], [7].

These results seem to show that the SPH method has the desired characteristics of convergence, at least for polytropic EOS.

Of course, one of the most important requirement for the method to work well is providing a good evaluation of the force field.

Usually, in the simulations, the regularization kernels have compact support (to reduce the computational cost) and their widths are such that every particle interacts with an almost constant and a priori fixed number of neighbours. It is found that this evaluation strongly depends on the size of the kernels.

In this paper we attempt to give a better way to establish, through a quantitative check of the error, a correct size of the kernels for a good evaluation of the force field, in the class of the cubic spline kernels. Actually, the spline kernels introduced and discussed by Monaghan and Lattanzio [8], are the most used in numerical simulations.

In what follows we shall denote with  $\nabla$  or  $\nabla_{\mathbf{r}}$  the usual symbolic vector of components  $\frac{\partial}{\partial x}, \frac{\partial}{\partial y}, \frac{\partial}{\partial z}$ , while the symbol  $*$  represent the usual convolution operator in  $\mathbb{R}^3$ . The points in the space will be denoted by  $\mathbf{r}$  and  $r \equiv |\mathbf{r}|$ .

## 2. SPH approximation of the fluid equations

### 2.1 The free case

A particle method to simulate the dynamical and thermodynamical evolution of a fluid corresponds to a direct discretization of the Lagrangian set of fluid-dynamical equations. In the case, for instance, of a barotropic compressible fluid without body forces this set writes as

$$\left\{ \begin{array}{l} \frac{d\rho}{dt} + \rho \nabla \cdot \mathbf{v} = 0 \\ \frac{d\mathbf{v}}{dt} + \frac{\nabla P}{\rho} = 0 \\ P = P(\rho). \end{array} \right. \quad (1)$$

In the SPH scheme the fluid, whose total mass is  $M$ , is represented by an

ensemble of  $N$  particles with masses  $m_i$  ( $i = 1, \dots, N$ ) such that  $\sum_i m_i = M$ , centered at points  $\mathbf{r}_i$ ;  $\{\mathbf{r}_i\}$  is a set of space points sampling the volume occupied by the fluid. To each particle is associated a density function called “kernel”. The most commonly used kernel is the third order spline function (see [8])

$$\phi(\mathbf{r}, h) = \frac{1}{\pi h^3} \begin{cases} 1 - (3v^2/2) + (3v^3/4) & \text{if } 0 \leq v \leq 1 \\ (2 - v)^3/4 & \text{if } 1 \leq v \leq 2 \\ 0 & \text{elsewhere} \end{cases} \quad (2)$$

where  $v = r/h$ . The width of the kernel,  $2h$ , is the radius of the spherical “fluid particle”; this radius may change particle by particle.

In SPH the pressure field per unit mass in the Euler equation is usually approximated by

$$\left(\frac{\nabla P}{\rho}\right)_{SPH}(\mathbf{r}_i) = \sum_{j=1}^N \left(\frac{P(\rho_i)}{\rho_i^2} + \frac{P(\rho_j)}{\rho_j^2}\right) \nabla\phi(\mathbf{r}_i - \mathbf{r}_j, h_i), \quad (3)$$

where

$$\rho_i \equiv \rho(\mathbf{r}_i) = \sum_{j=1}^N m_j \phi(\mathbf{r}_i - \mathbf{r}_j, h_i) \quad (4)$$

is the SPH approximation to the fluid mass density.

The density (4) evolves in time because the particles move under the Newton law

$$\ddot{\mathbf{r}}_i = - \left(\frac{\nabla P}{\rho}\right)_{SPH}(\mathbf{r}_i) \quad i = 1, \dots, N \quad (5)$$

which is the SPH version of the momentum equation in the system (1).

## 2.2 The self-gravitating case

SPH methods developed mainly in Astrophysics, due to its ability to handle fully 3D situations. Most of astrophysics simulations should necessarily include self-gravity. The system of equations underlying the motion of

barotropic self-gravitating fluids is a little more complicated than (1):

$$\left\{ \begin{array}{l} \frac{d\rho}{dt} + \rho \nabla \cdot \mathbf{v} = 0 \\ \frac{d\mathbf{v}}{dt} + \frac{\nabla P}{\rho} - \nabla U = 0 \\ \nabla \cdot \nabla U = -4\pi G \rho \\ P = P(\rho) \end{array} \right. \quad (6)$$

where  $G$  is the gravity constant. Due to the spherical symmetry of the kernels and Newton theorems, the SPH approximation of the gravitational force field is simply:

$$(\nabla U)_{SPH}(\mathbf{r}_i) = - \sum_{j=1}^N 4\pi G \frac{(\mathbf{r}_i - \mathbf{r}_j)}{|\mathbf{r}_i - \mathbf{r}_j|^3} \int_0^{|\mathbf{r}_i - \mathbf{r}_j|} \phi(x, h_i) x^2 dx \quad (7)$$

This SPH approximation is quite accurate, and numerical simulations show that the gravitational field is always fitted better than the pressure one (because of that the sum in (7) is usually substituted by a further approximation as in the P3MSPH code suggested by Monaghan and Lattanzio [8] or in TREESPH code proposed by Hernquist and Katz [9]). It is easy to convince oneself about that when considering the different nature of the pressure and gravitational fields. The first depends on the local distribution of the matter, and so it is strongly subject to the local fluctuations of the particle distribution, while the second rather depends on the global matter density. This is the reason why, in a particle scheme, it is easier to fit the gravitational force field than the pressure one.

So, in this paper we will focalize our attention on the SPH approximation of the pressure field, only.

### 2.3 Evaluating the error

The  $h$  value determines the number of particles which give an effective contribution in the sums (3) and (4), that is the number of neighbouring particles that effectively interact (touch) with the given one. This means that the effective pressure force strongly depends on  $h$ : a small  $h$  means a steep  $\phi$  profile in (2) and a small number of particle contributing to the sums, and viceversa for large  $h$ . It is easy to verify the two limits:

$$\lim_{h \rightarrow 0} \left( \frac{\nabla P}{\rho} \right)_{SPH}(\mathbf{r}) = 0 \quad \lim_{h \rightarrow \infty} \left( \frac{\nabla P}{\rho} \right)_{SPH}(\mathbf{r}) = 0. \quad (8)$$

In the common case of a polytropic EOS ( $P \propto \rho^\gamma$ ) the second limit holds just for  $\gamma > 2/3$ . It is so quite clear how the kernel size  $h$  is crucial to give a good SPH approximation of the pressure force field so that the particles, fluid-representatives, move on the correct trajectories (which are the characteristics of the fluid).

A quite natural way to determine a “best” local value of  $h$  is through the minimization of the absolute value of the relative error

$$E_r(\mathbf{r}; h) = \frac{\left| \left( \frac{\nabla P}{\rho} \right) (\mathbf{r}) - \left( \frac{\nabla P}{\rho} \right)_{SPH} (\mathbf{r}) \right|}{\left| \left( \frac{\nabla P}{\rho} \right) (\mathbf{r}) \right|} \quad (9)$$

At a given particle configuration, for fixed  $\mathbf{r}$ ,  $E_r$  depends on  $h$  only.

If we set the unitary vectors  $\mathbf{n}_e(\mathbf{r}) = (\frac{\nabla P}{\rho}) / |\frac{\nabla P}{\rho}|$  (the exact direction) and  $\mathbf{n}_a(\mathbf{r}) = (\frac{\nabla P}{\rho})_{SPH} / |\frac{\nabla P}{\rho}|_{SPH}$  (the approximated SPH direction) the relative error (9) can be rewritten as

$$E_r(\mathbf{r}; h) = \left| (\mathbf{n}_e - \mathbf{n}_a) + \frac{|\frac{\nabla P}{\rho}| - |\frac{\nabla P}{\rho}|_{SPH}}{|\frac{\nabla P}{\rho}|} \mathbf{n}_a \right| \quad (10)$$

This obvious identity suggests us to split the relative error into a *direction* error  $E_{dir}$  and a *modulus* error  $E_{mod}$ . Respectively

$$E_{dir}(\mathbf{r}; h) = |\mathbf{n}_e - \mathbf{n}_a|, \quad E_{mod}(\mathbf{r}; h) = \left| \frac{|\frac{\nabla P}{\rho}| - |\frac{\nabla P}{\rho}|_{SPH}}{|\frac{\nabla P}{\rho}|} \mathbf{n}_a \right| \quad (11)$$

### 3. A model for comparing exact and SPH pressure fields

To test the sensitivity of the SPH approximation of the force field on the kernel width, we will consider particle distributions sampled from the family of Plummer’s density laws [10]:

$$\rho(r) = \frac{\rho_0}{\left[ 1 + (r/r_c)^2 \right]^{5/2}}. \quad (12)$$

The law (12) is often used in theoretical Astrophysics because it is a good 2-parameter ( $\rho_0$  and  $r_c$ ) fit to many self-gravitating objects (globular clusters,

roundish elliptical galaxies, etc.). Here it is used just as a reference density law apt to simulate a range of different density and pressure gradients. To do this one can change the central density  $\rho_0$  and the length scale  $r_c$ ; increasing  $r_c$  means dilute the distribution (smoothing the gradients).

We fix the total mass of the sphere,  $M$  so that the central density  $\rho_0$  is linked to the characteristic length scale  $r_c$  which is our second free parameter. As we said, in the SPH scheme the density is represented by an ensemble of  $N$  particles with masses  $m_i$  and positions  $\mathbf{r}_i$  ( $i = 1, \dots, N$ ). In this scheme the pressure field in the  $\mathbf{r}_i$  position can be approximated by (3). The particle distribution sampling the regular density (12) is obtained choosing first a set of random particle positions  $\bar{\mathbf{r}}_i$  according to a uniform probability law in a sphere and then replacing every  $\bar{\mathbf{r}}_i$  by  $\mathbf{r}_i$  such that

$$\int_0^{r_i} \rho(s) s^2 ds = \frac{\bar{r}_i^3}{3}. \quad (13)$$

In our simulations we shall use 10,000 particles of individual mass  $m_i = M/10,000$ .

An interesting quantity associated to  $h$  is the number of particles which give an effective contribution in the sums (3) and (4), that is the number of particles that effectively interact with the given one. In practical simulations, this number is usually set to a constant value, the same for every particle.

Due to the spherical symmetry of our model, the directional part of the relative error  $E_{dir}$  is a decreasing function of  $h$ , and is obviously minimized taking  $h$  as large as possible (which is computationally expensive), while the error in the absolute value  $E_{mod}$  is not a monotonic function of  $h$  (see eq.(8)). So, it is quite natural to study the modulus part of the error separately.

### 3.1 The results

We have studied the minimization of the relative error  $E_r$ , as a function of  $h$  (assumed to be the same for each particle) for three different values of  $r_c$  in (12), namely 0.25, 0.5, 1. For  $\gamma$  the values 7/5, 5/3 and 2, of clear physical interest, are considered.

For each case the minimization of  $E_r$  as function of  $h$  has been performed on a set of 100 different particle positions. To do that we evaluate the

pressure field on each particle using the same kernel for all the particles, then we modify the size of this kernel to obtain the best result.

Figs 1 and 2 show (for some  $r_c$  and  $\gamma$ ) the minimum relative error  $E_r$  as function of the distance from the centre and the number of particles (neighbours) within the kernel of any of the 100 particles, respectively.

These figures seem to show that the best results (low value for  $E_r$  coupled with a small number of neighbours) have been obtained in the middle radius zone. The minimum error  $E_r$  is, in the average, a slightly decreasing function of  $r$ .

To study better the behaviour of the  $E_r$  function, we have done a separate statistics of the modulus ( $E_{mod}$ ) and directional ( $E_{dir}$ ) errors. We have considered 30 particles in three different regions, around  $r/r_c = 0, 1, 2$ , assuming, in the state law,  $\gamma = 5/3$ . To give a visual idea of the quality of the SPH approximation, in Figs 3, 4, 5 the SPH pressure field is compared with the exact one. For graphical convenience, for each particle we have plotted the exact vector and a vector whose modulus is given by the best SPH approximation (that given by  $E_r$  minimization) at an angle, clockwise oriented, given by the scalar product between the exact,  $\mathbf{n}_e$ , and SPH,  $\mathbf{n}_a$ , unitary vectors in space (cp. Sect. 2.3). The exact vector points to the centre; in the figures the centre is assumed to be at an infinite distance. It is quite evident the better field direction approximation for larger  $r_c$  and  $r/r_c$  (i.e. less steep gradients).

To give a more precise measure of the errors, in Figs 6, 7, 8 we have plotted the relative error  $E_r$  and the modulus error  $E_{mod}$ . The number of neighbours and, to give a measure of the direction error  $E_{dir}$ , the cosine of the angle  $\Theta$  between the SPH and exact vector fields ( $\cos \Theta = \mathbf{n}_e \cdot \mathbf{n}_a$ ) have also been plotted. Figs 6 – 8 show that the field is well approximated in the middle zone while a very good approximation of just the direction of the pressure field is obtained in the outer one. The best balancing of the two errors have been obtained in the middle zone. In the inner zone, where the pressure gradient should almost vanishing, the approximation is critically dependent on sampling problems (see discussion in Sect. 4.).

The different radial behaviours of the errors  $E_r$ ,  $E_{mod}$  and  $E_{dir}$ , suggest us to split the **evaluation** of SPH approximation in two parts: first we fix  $h$  to evaluate at best the modulus of the pressure field, then we enlarge it to obtain an acceptable direction of the field with a computationally reasonable number of neighbours.



To this scope, for several particles positioned at different radii, we have plotted the errors  $E_r$ ,  $E_{mod}$  and  $E_{dir}$  as functions of  $h$ . These plots, Fig.9, show that the best error in the pressure field absolute value ( $E_{mod}$ ) is reached with a smaller  $h$  value than when the global error ( $E_r$ ) was minimized.

Taking into account these results, we suggest to estimate separately the modulus and the direction of the pressure field using two different kernel widths, as aforementioned. The first width, say  $h_{mod}$ , is obtained through the minimization of the modulus error  $E_{mod}$ , the second,  $h_{dir}$ , is taken proportional to the first in a way to keep the error in direction  $E_{dir}$  below an acceptable limit.

To set such proportionality constant, we evaluate, for any particle in the three regions considered before, the quantity  $E_{dir}$  as function of the variable  $h/h_{opt}$ , where  $h_{opt}$  is the width obtained minimizing the modulus error  $E_{mod}$ .

The plots in Fig. 10 have been obtained averaging the  $E_{dir}(h/h_{opt})$  functions found for each particle. The length of the vertical straight lines is proportional to the dispersion around the mean value.

This figure shows that it is sufficient to double the  $h_{opt}$  value to get a good (within 10%) approximation of the direction of the field. So a reasonable choice of the proportionality constant is 2.

In Figs 11, 12, 13 comparisons of the results obtained following this recipe compared with those obtained by the simple minimization of  $E_r$  are shown. In these figures the number of neighbours corresponding to  $h_{opt}$  and the percentage global error  $E_r$  are plotted for all particles in the three zones before considered for  $r_c = 0.25, 0.5, 1$ , respectively, and  $\gamma = 5/3$ . The figures show that  $h_{opt}$  is associated to an almost constant number of neighbour particles, which corresponds to about 10% of the total number. This behaviour occurs in all the cases here considered.

Note that usual SPH implementations evaluate the pressure field using kernels with a size such that the number of neighbouring particles is set to a given constant. Thus, we tested the computational cost of the implementation here proposed by comparing the CPU times (on a DEC Alpha 200 4/233) required to evaluate the pressure field by the usual and our SPH method.

We have fixed the number of neighbouring particles to compute the absolute value of the pressure gradient to 10% of the total, as suggested by our  $E_{mod}$  minimization. This fraction corresponds to a certain kernel size, and to evaluate the direction of the field we double this size. In the usual method just one kernel size is used (here we choose the one giving 10% neighbours).

As expected, the computational cost of a double-kernel evaluation of the pressure field is  $\approx 1 + 2^3$  times the single-kernel one, which is the price of the good improvement of the error.

For the sake of a good balance between computational weight and precision we tried  $h_{dir} = \sqrt[3]{2}h_{mod}$ , i.e. the size needed to almost double the number of neighbours. This case requires a computational cost which is of the order of  $1 + 2$  times the single-kernel method with  $h = h_{mod}$ , with a lower error level; to have a similar approximation we verified that  $h_{mod}$  is allowed to be  $< h$  thus to give a ratio of CPU times less than 2. Being this part of SPH evaluation wholly parallelizable explains why in this way we can obtain a better approximation waiting the same solar time.

#### 4. Comparing SPH and Monte-Carlo methods

The basic idea of the SPH method is to “reconstruct” a function  $f$ , whose values are known in some “particle” points, by interpolation (in fluid-dynamical applications the particles are distributed to fit the fluid mass density). The way SPH does that is through a Monte-Carlo approximation of the convolution integral  $f * \phi$ , where  $\phi$  is a regular kernel function. The function  $f * \phi$  is close to  $f$  if  $\phi$  is close to the Dirac’s delta. In the same way it is possible to reconstruct  $\nabla f$ . Indeed, by noting that  $(\nabla f) * \phi = f * (\nabla \phi)$ , we can evaluate the latter integral, instead of the first, through the knowledge of  $f$  only. A similar procedure may be used for any derivative of  $f$  with respect to space variables.

Monte-Carlo methods are the most studied and the most advanced particle methods in numerical analysis, so it is quite natural to compare the SPH approximation method with direct Monte-Carlo ones.

While we refer the reader to a forthcoming paper [11] for a more detailed and accurate analysis of the link between SPH and Monte-Carlo approximation methods, for the purposes of this paper we limit here ourselves to show the difference between the SPH and the Monte-Carlo interpolations for the pressure force field only.

As we said in previous Sections, the pressure force field  $\nabla P/\rho$  is the most delicate term to handle in fluid-dynamical simulations. In SPH,  $\nabla P/\rho$  is usually approximated by eq.(3). The Monte-Carlo rule, choosing  $\rho$  as

distribution function of the particles, gives

$$\left(\frac{\nabla P}{\rho}\right)_{MC}(\mathbf{r}) = \frac{1}{N} \sum_i \frac{\nabla P(\mathbf{r}_i)}{\rho^2(\mathbf{r}_i)} \phi(\mathbf{r} - \mathbf{r}_i, h), \quad (14)$$

where we assume  $h_i = h$  for any  $i$ . The average value, over the particle configuration space, of the sum in the right hand side of eq.(14) gives the exact pressure field  $(\nabla P/\rho)(\mathbf{r})$ . On the contrary, averaging the SPH approximation sum (3) we find

$$\left\langle \left(\frac{\nabla P}{\rho}\right)_{SPH} \right\rangle(\mathbf{r}) = \left(\frac{\nabla P}{\rho}\right)(\mathbf{r}) + \int \left(\frac{P(\mathbf{r})}{\rho^2(\mathbf{r})} - \frac{P(\mathbf{r}')}{\rho^2(\mathbf{r}')}\right) \nabla \rho(\mathbf{r}') \phi(\mathbf{r} - \mathbf{r}', h) d^3 \mathbf{r}', \quad (15)$$

the value of the integral being zero if  $P \propto \rho^2$ , otherwise it goes to zero with  $h$  whenever the functions  $\nabla P/\rho^2$  and  $\nabla \rho$  are regular enough (for example if they are differentiable). This means that the SPH scheme (without artificial viscosity) may not be apt to represent extreme situations, as when, for example, shock fronts occur (i.e. when a discontinuity on the density occurs).

Now, it is easy to show that the difference  $\Delta$  between the Monte-Carlo and SPH sums writes as

$$\begin{aligned} \Delta = & \frac{1}{N} \sum_i \left[ \nabla_{\mathbf{r}'} \left( \frac{P(\mathbf{r}')}{\rho^2(\mathbf{r}')} \phi(\mathbf{r} - \mathbf{r}', h) \right) \right]_{\mathbf{r}'=\mathbf{r}_i} + \\ & \frac{2}{N} \sum_i \frac{P(\mathbf{r}_i)}{\rho^3(\mathbf{r}_i)} \nabla \rho(\mathbf{r}_i) \phi(\mathbf{r} - \mathbf{r}_i, h) - \frac{1}{N} \sum_i \frac{P(\mathbf{r})}{\rho^2(\mathbf{r})} \nabla_{\mathbf{r}} \phi(\mathbf{r} - \mathbf{r}_i, h) \end{aligned} \quad (16)$$

and its average value is not zero, as we said.

This term is too difficult to handle in general situations. But we can study it in some simple cases. For example, for a fluid which state law is  $P \propto \rho^2$ , then eq.(16) reduces to

$$\Delta = \frac{2}{N} \sum_i \frac{1}{\rho(\mathbf{r}_i)} \nabla_{\mathbf{r}_i} (\rho(\mathbf{r}_i) \phi(\mathbf{r} - \mathbf{r}_i)). \quad (17)$$

In a situation not far from spatial uniformity ( $|\nabla \rho|/\rho \ll 1$ ), eq.(17) reduces to:

$$\Delta \simeq \frac{2}{N} \sum_i \nabla_{\mathbf{r}_i} \phi(\mathbf{r} - \mathbf{r}_i), \quad (18)$$

whose averaged value is the vector  $-\nabla\rho$ . On the other hand, if we suppose  $|\nabla\rho|/\rho \gg 1$

$$\Delta \simeq \frac{2}{N} \sum_i \frac{\nabla_{\mathbf{r}_i} \rho(\mathbf{r}_i)}{\rho(\mathbf{r}_i)} \phi(\mathbf{r} - \mathbf{r}_i) \quad (19)$$

holds, and the averaged value of the right hand term is the vector  $\nabla\rho$ .

The first case should be the better one, anyway when the density profile is quasi-constant, the fluctuations due to the particle fit amplify the relative error.

Let us consider now the state law  $P \propto \rho^{2+\alpha}$  where  $\alpha > 0$ . When  $\ln^2(\rho) \max(1, \rho^{-\alpha}) \ll 1$  we have  $P \simeq \rho^2(1 + \alpha \ln(\rho))$ , and (16) writes as

$$\begin{aligned} \Delta \simeq & \frac{2}{N} \sum_i \frac{1}{\rho(\mathbf{r}_i)} \nabla_{\mathbf{r}_i} (\rho(\mathbf{r}_i) \phi(\mathbf{r} - \mathbf{r}_i)) + \\ & \frac{2\alpha}{N} \sum_i \nabla_{\mathbf{r}_i} [\ln(\rho(\mathbf{r}_i)) \phi(\mathbf{r} - \mathbf{r}_i)] + \frac{\alpha}{N} \sum_i \phi(\mathbf{r} - \mathbf{r}_i) \nabla_{\mathbf{r}_i} \ln^2(\rho(\mathbf{r}_i)). \end{aligned} \quad (20)$$

Let us study again the two extreme cases  $|\nabla\rho|/\rho \ll 1$  and  $|\nabla\rho|/\rho \gg 1$ . It is easy to convince ourselves that the previous considerations still hold, but only if  $|\ln\rho|$  is not too great. This means, for example, that SPH approximation is not expected to be accurate near the boundaries of the fluid.

In conclusion, the best SPH fit (i.e. comparable with Monte-Carlo one) for the pressure field can be obtained when both the following conditions hold:

i) the density is not too large or too small and ii) it has a profile along a well defined direction with small gradients.

Moreover, we notice that the previous analysis does not depend on the overall mass distribution but only on its local behaviour. Then the conditions i) and ii) are valid criteria in very general situations.

Let us now apply previous considerations to the spherical model studied in this paper. The results of our simulations, shown in Sect. 3, confirm the expectations based on the previous analysis: the best results on the evaluation of the pressure field are obtained in those zones of the model where the conditions i) and ii) approximately hold, i.e. in the central ones as suggested by the density law (12) and

$$\frac{|\nabla\rho|}{\rho} \propto \frac{r}{(r^2 + r_c^2)} \quad (21)$$

Moreover, comparing models with different characteristic radii we found that the precision increases as  $r_c$  grows, as suggested by

$$\max_r \frac{|\nabla\rho|}{\rho} \propto \frac{1}{r_c}. \quad (22)$$

## 5. Conclusions

In this paper we have studied the error in the SPH evaluation of the pressure field for the set of polytropic compressible fluids in spherical symmetry. The spherical symmetry allows us to compare SPH evaluation with a simple model, saving the confidence that the main results are still valid in more general and realistic situations, as we have shown with analytical considerations in Sect.4. First we determined the kernel sizes which minimize the global error  $E_r$  (see eq.(9)); they depend on the particle positions becoming narrower where the density is lower, due to that in external regions the right (radial) direction of the field is easily obtained. This latter is linked to that a good approximation of the pressure field is harder to be obtained in very central and peripheral regions. Actually, in very central zones, where  $|\nabla P|/\rho \simeq 0$  and  $|\nabla\rho|/\rho \ll 1$ , to get an acceptable fit of the pressure field direction so large kernel sizes are needed to make the SPH pressure gradient underestimated. On the contrary, in the outer regions, the radial direction of the field is well fitted even with small kernel sizes (i.e. few neighbours): this implies a certain overestimate of the pressure gradient.

All this has suggested us to study separately the behaviours of the modulus and directional error, as defined by eq. (11).

Given that the larger the kernel the better the approximated direction, we minimized the error in modulus  $E_{mod}$  rather than the global one.

The obtained kernel width slightly depends on the particle position thus an almost constant number of neighbours is needed to perform the best approximation. In our simulations this number is found to be 10% of the total independently of the particle positions and the characteristic radius of the model.

Moreover, a good (giving an error less than 10%) direction of the pressure field is obtained doubling that kernel size. Unfortunately, this evaluation requires a CPU time almost 8 times the one required by the single-kernel

evaluation. We have obtained a good balance between the quality of approximation and the CPU weight fixing the ‘direction’ kernel to be  $\sqrt[3]{2}$  times the ‘modulus’ one.

So, a good prescription to estimate the pressure field in SPH is to evaluate the absolute value of the field with a kernel size giving a constant number of neighbouring particles, while the direction is estimated using another kernel size as described before.

The CPU time required by this procedure is less than two times that required by the usual (single-kernel) SPH evaluation of the pressure field. This recipe becomes convenient when a parallelized code is used.

## References

1. Lucy, L., *Astron. J.*, **82**, 1013 (1977).
2. Gingold, R.A., Monaghan, J.J., *Mon. Not. Roy. Astron. Soc.*, **181**, 375 (1977).
3. Monaghan, J.J., *Ann. Rev. of Astron. and Astroph.*, **30**, 543 (1992).
4. Oelschläger, K., *Arch. Rat. Mech. An.*, **115**, 297 (1991).
5. Di Lisio, R., *Mat. Met. Appl. Sci.*, **18**, 1083 (1995).
6. Di Lisio, R., Grenier, E. and Pulvirenti, M., *Special Issue devoted to Simulations Methods in Kinetic Theory*, Computers and Mathematics with Applications, in press (1996).
7. Di Lisio, R., Grenier, E. and Pulvirenti, M., *Annali della Scuola Normale di Pisa*, in press (1996).
8. Monaghan, J.J., Lattanzio, J.C., *Astron. Astrophys.*, **149**, 135 (1985).
9. Hernquist, L., Katz, N., *Ap. J. Suppl.*, **70**, 419 (1989).
10. Plummer, H.C., *Mon. Not. Roy. Astron. Soc.*, **71**, 460 (1911).
11. Capuzzo-Dolcetta, R., and Di Lisio, R., in preparation.

## Figure captions

### Fig. 1

For the Plummer's sphere with  $r_c = 0.25$ , and polytropic exponent  $\gamma = 7/5$  (solid line) and  $\gamma = 2$  (dashed line) panel (a) shows the minimum relative error  $E_r$  (in percent) vs. the radial coordinate and panel (b) the corresponding relative percentage number of neighbouring particles  $N_n$  (see text).

### Fig. 2

As in Fig.1 but  $r_c = 1$ .

### Fig. 3

For the polytropic exponent  $\gamma = 5/3$ , the exact (vertical arrows) and approximate  $\nabla P/\rho$  fields are shown in three different radial zones, for  $r_c = 0.25$ .

### Fig. 4

As in Fig.3 but for  $r_c = 0.5$

### Fig. 5

As in Fig.3 but for  $r_c = 1$ .

### Fig. 6

For the polytropic exponent  $\gamma = 5/3$  and  $r_c = 0.25$ , we show, from bottom up:

- the minimum relative error  $E_r$  in percentage;
- the corresponding modulus error  $E_{mod}$  in percentage;
- the cosine of the angle  $\Theta$  between the unitary vectors  $\mathbf{n}_a$  and  $\mathbf{n}_e$  (see text);
- the number of neighbours  $N_n$  in percentage to the total;

for all the 30 particles in each of the three chosen shells. Solid line refers to the inner ( $r/r_c = 0$ ) shell, dashed line to the middle ( $r/r_c = 1$ ) and dot-dashed to the outer ( $r/r_c = 2$ ).

### Fig. 7

As in Fig.6 but for  $r_c = 0.5$

### Fig. 8

As in Fig.6 but for  $r_c = 1$ .



### Fig. 9

For the polytropic exponent  $\gamma = 5/3$  and characteristic radius  $r_c = 0.5$ , the values of the errors  $E_r$  (solid lines),  $E_{mod}$  (dashed lines) and  $E_{dir}$  (dot-dashed lines) are plotted as functions of  $h/r_c$  for 10 particles positioned at different distances from the centre (as labelled).

### Fig. 10

For the polytropic exponent  $\gamma = 5/3$  and  $r_c = 0.25, 0.5, 1$  the averaged (over all the 30 particles in each shell) directional error  $E_{dir}$  as function of  $h/h_{opt}$  is plotted (see text). The lengths of the vertical straight lines are proportional to the dispersions of the data around the mean values.

### Fig. 11

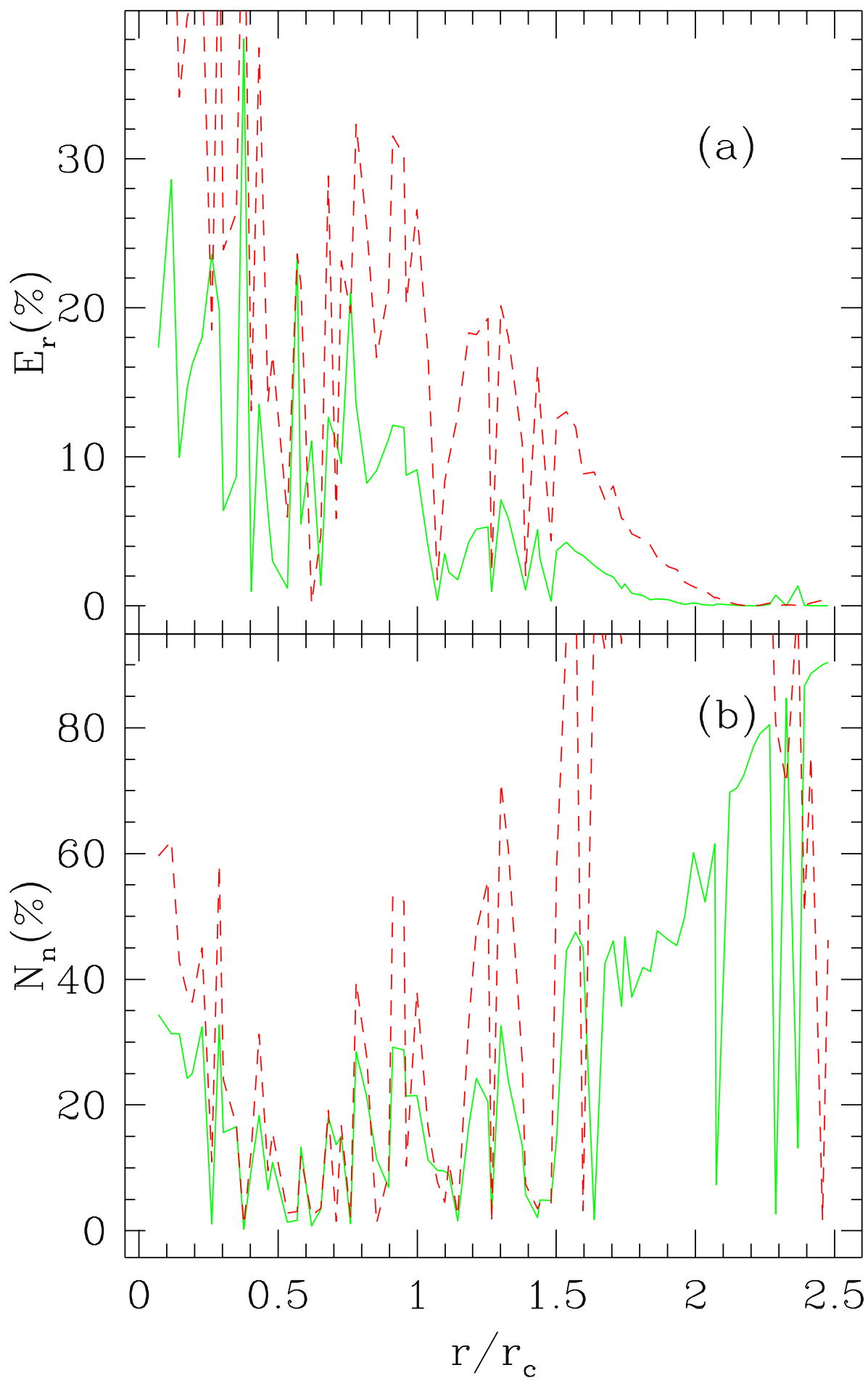
For the polytropic exponent  $\gamma = 5/3$  and  $r_c = 0.25$  the percentage number of neighbours  $N_n$  and the percentage total error  $E_r$  are shown for all the particles in the shells when our double-kernel method is applied (solid lines) and when  $E_r$  is minimized (dashed lines) for all the 30 particles in the shells (as labelled in the right panels). In each case the horizontal straight line correspond to the average value over all the 30 particles.

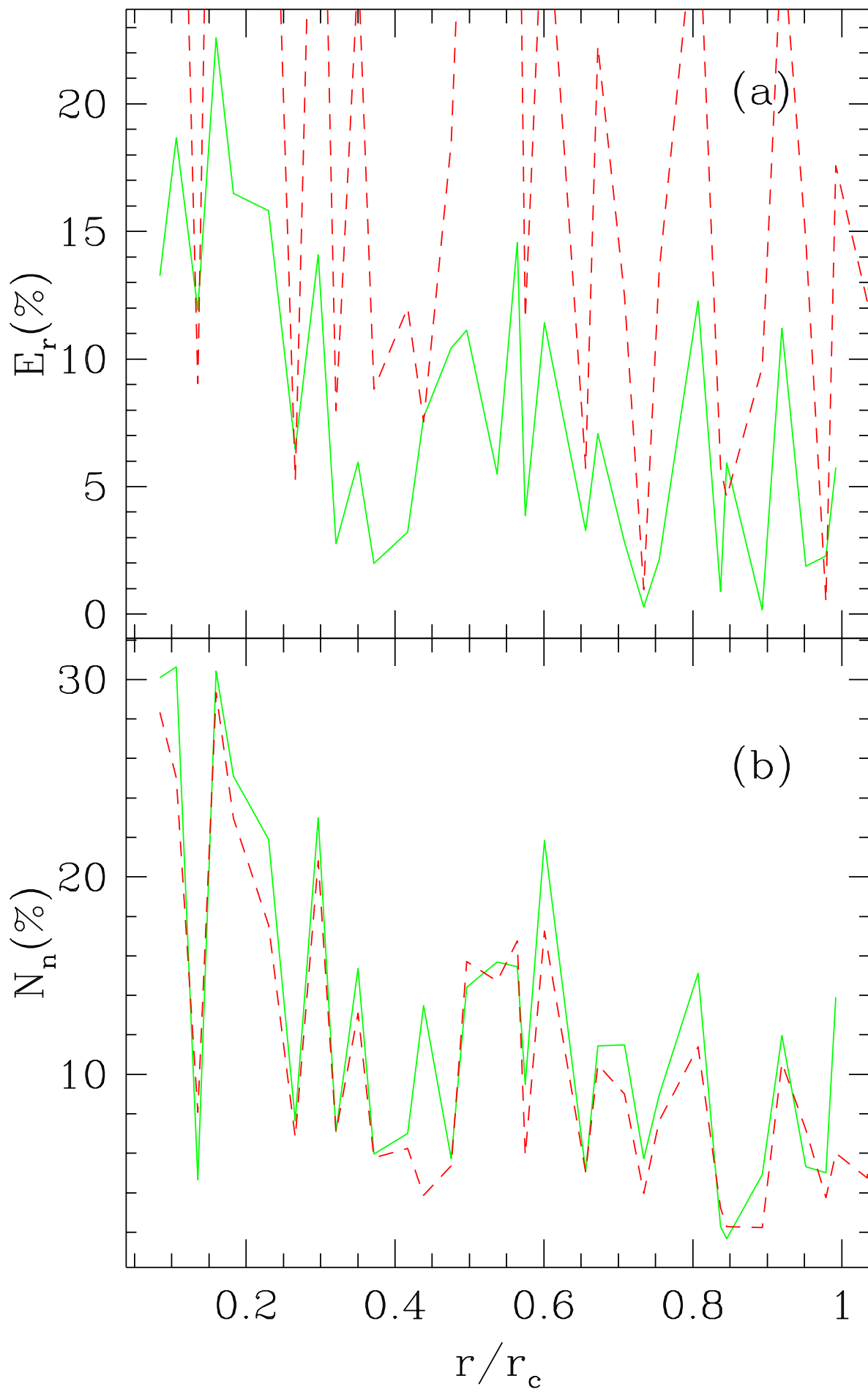
### Fig. 12

As in Fig.11 but for  $r_c = 0.5$

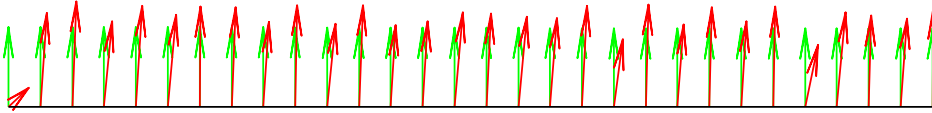
### Fig. 13

As Fig.11 but for  $r_c = 1$ .

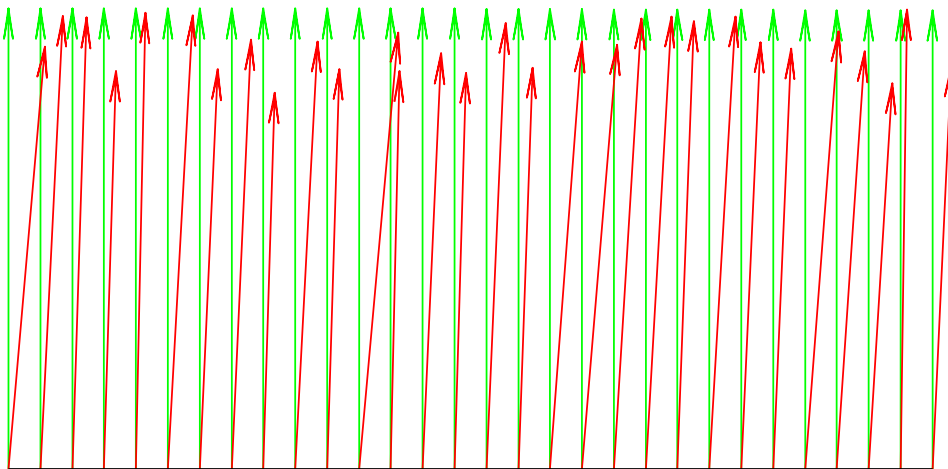




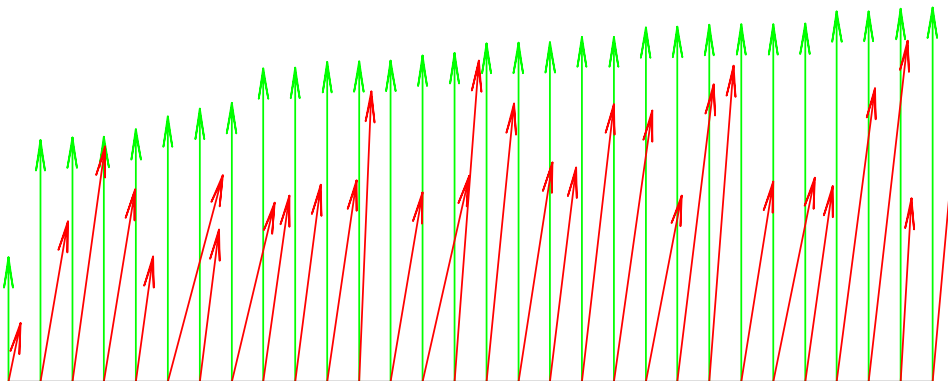
↑  
Toward the centre



$$r/r_c = 2$$

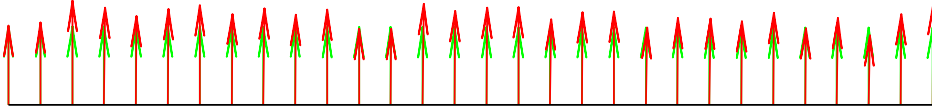


$$r/r_c = 1$$

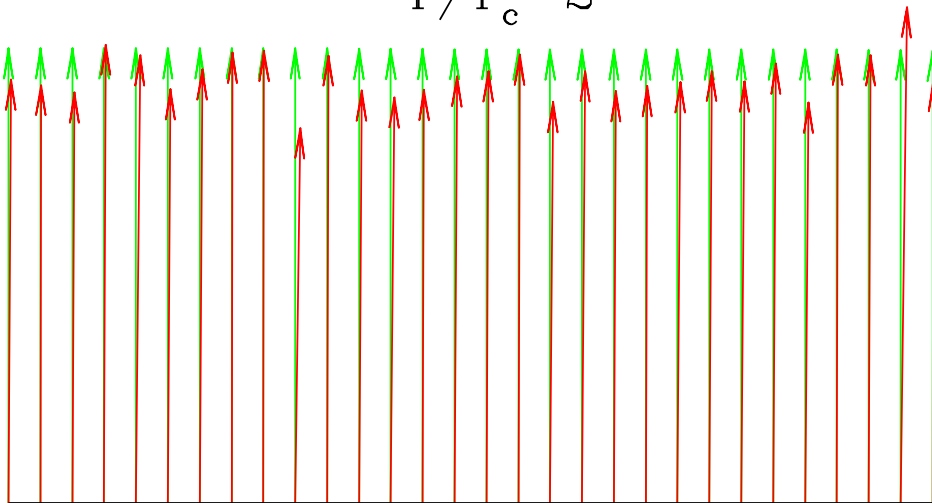


$$r/r_c = 0$$

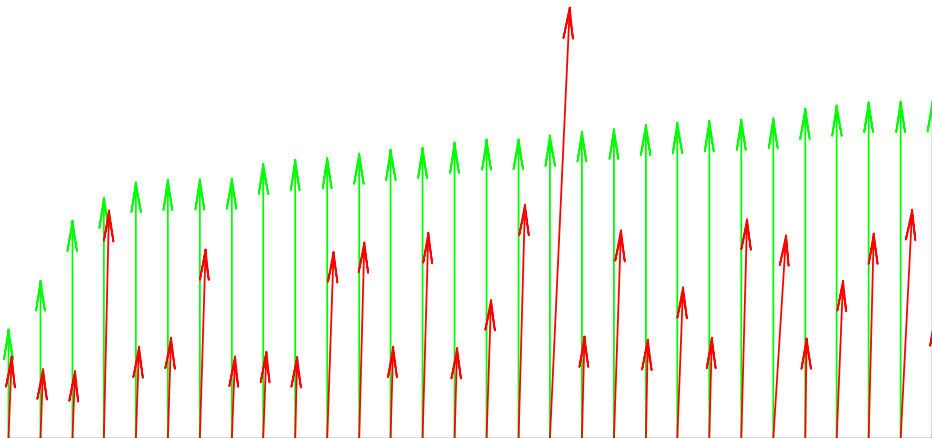
Toward the centre



$$r/r_c = 2$$

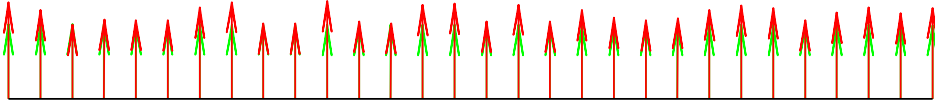


$$r/r_c = 1$$

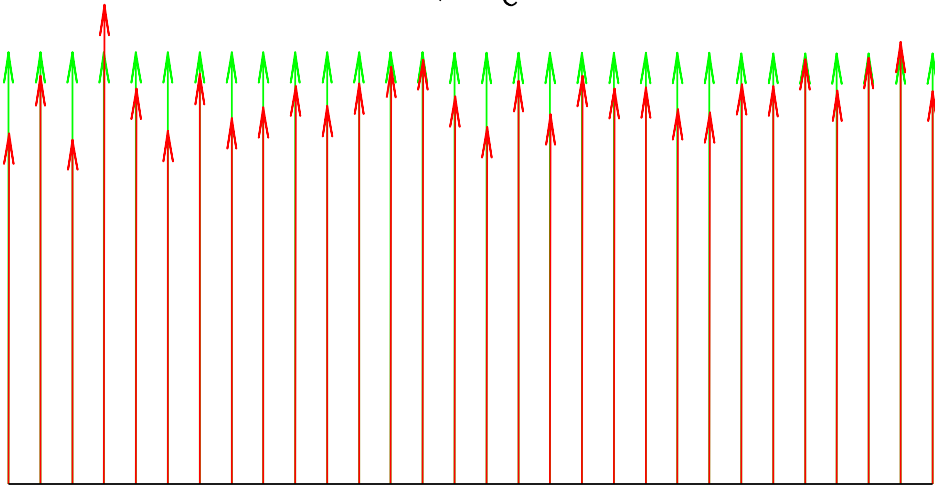


$$r/r_c = 0$$

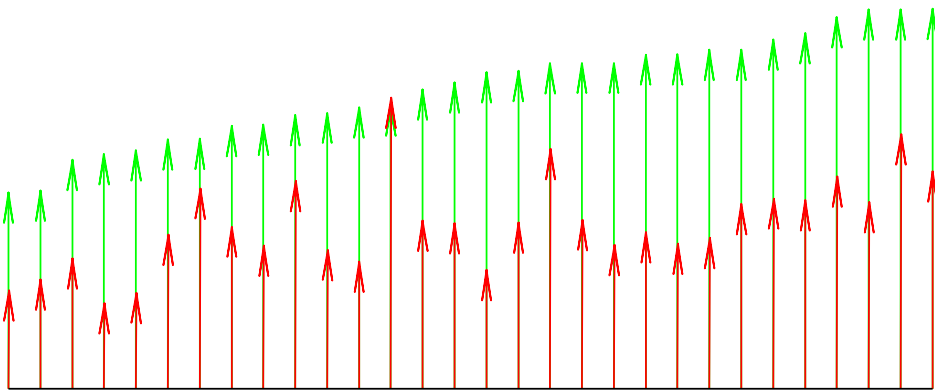
↑  
Toward the centre



$$r/r_c = 2$$



$$r/r_c = 1$$



$$r/r_c = 0$$

